Metaheuristic Color Scheme Strategies for Enhanced Visual Inspection of 3D IC Layouts

1st Jie Zhang
College of Design and Engineering
National University of Singapore
Singapore 117583
zhang_jie@u.nus.edu

2nd Zhansen Shi
College of Design and Engineering
National University of Singapore
Singapore 117583
shizhansen@u.nus.edu

3rd Hanchen Wang
College of Design and Engineering
National University of Singapore
Singapore 117583
Wang2406@e.ntu.edu.sg

4th Zhuoyang Zhang
College of Design and Engineering
National University of Singapore
Singapore 117583
e1525813@u.nus.edu

5th Lucas Lum
College of Design and Engineering
National University of Singapore
Singapore 117583
e190013@e.ntu.edu.sg

6th Quanhao Gan
College of Design and Engineering
National University of Singapore
Singapore 117583
e1351209@u.nus.edu

7th Shaoyu Cai
College of Design and Engineering
National University of Singapore
Singapore 117583
shaoyucai@nus.edu.sg

8th Eng Tat Khoo
College of Design and Engineering
National University of Singapore
Singapore 117583
etkhoo@nus.edu.sg

9th Yeow Kheng Lim
College of Design and Engineering
National University of Singapore
Singapore 117583
eleykl@nus.edu.sg

2025 IEEE Physical Assurance and Inspection of Electronics (PAINE) | 979-8-3315-6787-3/25/$31.00 ©2025 IEEE | DOI: 10.1109/PAINE66113.2025.11320224

***Abstract*—The increasing complexity of three-dimensional integrated circuits (3D ICs) poses significant challenges for visually distinguishing dense networks of embedded traces, hindering both manual inspection and AI-assisted analysis. The absence of a standardized trace color scheme further complicates failure analysis (FA), particularly with the rise of heterogeneous integration. To address this, we formulate trace coloring as a multi-objective optimization problem and evaluate seven metaheuristic color scheme strategies. The proposed Adaptive Elitist Particle Swarm Optimization (AEPSO) algorithm outperforms all other methods. It achieves a minimum intra-group color difference of 5.52, surpassing the just-noticeable difference (JND) threshold of 2.3, ensuring that colors within each group remain easily distinguishable to the human eye. In addition, we develop a virtual reality (VR) visualization framework to support immersive spatial inspection of 3D IC layouts.**

***Index Terms*—3D ICs, Color Scheme Optimization, Metaheuristic Algorithms, Failure Analysis, Virtual Reality.**

I. Introduction

As semiconductor integration continues to scale in complexity, visualizing and inspecting three-dimensional integrated circuits (3D ICs) has become increasingly challenging. With stacked dies, interconnects, and through-silicon vias (TSVs), engineers require precise color-coded layouts to identify signal traces and verify connectivity [1].

However, no standardized color scheme currently exists for 3D IC visualization. Traditional color scheme generation methods, including histogram-based techniques, clustering algorithms, and neural network methods [2], often fail to ensure perceptual distinguishability between closely packed or functionally distinct regions. This limitation becomes even more critical with the adoption of heterogeneous integration, which adds further complexity to failure analysis (FA) workflows and extends chip development cycles [3].

In this paper, we present a comparative study of metaheuristic-based color scheme strategies aimed at maximizing perceptual contrast and enhancing trace readability in 3D ICs. Among the seven evaluated metaheuristics, our proposed Adaptive Elitist Particle Swarm Optimization (AEPSO) consistently outperforms the other six conventional metaheuristics, achieving the highest overall performance. In particular, AEPSO yields a minimum intra-group color difference ($\Delta E_{min,intra}$) of 5.52, significantly surpassing the just-noticeable difference (JND) threshold of approximately 2.3 [4, p. 44], thereby ensuring clear perceptual separation within each color group. Notably, AEPSO provides a 24.6% improvement over the standard Particle Swarm Optimization (PSO), which represents the best-performing conventional method. The resulting color scheme is applicable across a range of data representations, including empirical 3D reconstructions from layout data, 3D X-ray tomography, and simulated structural models [5], thereby maintaining visual coherence across both experimental and design domains.

To facilitate perceptual evaluation, we further develop a virtual reality (VR) framework for immersive inspection of optimized 3D IC layouts. This integrated approach supports more effective FA and has the potential to accelerate design verification in advanced packaging.

II. Background and Related Work

A. Color Space

Color space is a vector space with three or more parameters, representing colors as human perceptions of visible light (400–700 nm) [6].

Red-Green-Blue (RGB) color space is a classic model widely used in displays. The standard RGB (sRGB) model adds gamma correction to reduce device dependency by addressing nonlinear input-luminance relations [7].

The *Commission Internationale de l'Éclairage* (CIE) proposed CIE 1931 XYZ space, defining XYZ via a linear RGB transformation [8]. To improve perceptual uniformity, it later introduced CIE 1976 L*u*v* (CIELUV) and CIE 1976 L*a*b* (CIELAB), both derived through nonlinear transformations of XYZ [9].

Hue-Chroma-Lightness (HCL) space, or polar LAB, is a polar form of CIELAB, expressing a* and b* as hue angle (H) and chroma (C) [9]:

$$H = \arctan\left(\frac{b^*}{a^*}\right), \quad C = \sqrt{a^{*2} + b^{*2}} \tag{1}$$

HCL color space is used in this paper to select color codes, offering perceptual uniformity and interpretability.

B. Color Difference

Color difference (ΔE) quantifies the perceived difference between two colors. As large differences are less relevant, most research focuses on small color differences, often using just-noticeable difference (JND).

The majority of ΔE formulas are based on CIELAB space:

- ΔE^*_{ab} (CIE76): Uses Euclidean distance in CIELAB.
- ΔE^*_{94} (CIE94): Enhances the accuracy of ΔE^*_{ab} by incorporating weighting factors for hue, chroma, and lightness differences.
- ΔE_{00} (CIEDE2000): Refines weighting functions to address perceptual non-uniformities, particularly in low-chroma and skin-tone regions. The final calculation is as follows [10]:

$$\Delta E_{00} = \left[\left(\frac{\Delta L'}{k_L S_L}\right)^2 + \left(\frac{\Delta C'}{k_C S_C}\right)^2 + \left(\frac{\Delta H'}{k_H S_H}\right)^2 + R_T \left(\frac{\Delta C'}{k_C S_C}\right)\left(\frac{\Delta H'}{k_H S_H}\right)\right]^{1/2} \tag{2}$$

where $\Delta L'$, $\Delta C'$, and $\Delta H'$ are the adjusted lightness, chroma, and hue differences; S_L, S_C, and S_H are weighting functions; k_L, k_C, and k_H are parametric factors; and R_T accounts for chroma–hue interaction.

ΔE_{00}, the current CIE standard, is used in this paper to assess perceptual color differences.

C. Color Scheme Generation Methods

Color schemes can be generated using two main approaches: manual design and computer-automated generation.

1) Manual Design

Assigning color manually to individual traces relies on designers' subjective judgment and color theory [11], using color guides and designing tools such as HCL color space and Pantone chart [12].

2) Computer-Automated Generation

Computer-automated generation methods include:

- Histogram-based methods: Convert the color information of image pixels into a histogram and identifies the most frequent colors as the dominant colors [13].
- Clustering-based methods: Divide the color space into distinct regions by grouping similar colors into compact clusters.
- Metaheuristic methods: Employ metaheuristics to search for optimal or near-optimal solutions [14].
- Neural network methods: Leverage deep learning architectures to extract color features and generate customizable schemes.

Histogram methods often ignore brightness, misaligning dominant colors with perception. Clustering is efficient but lacks perceptual uniformity. Neural networks face challenges in data preparation and complexity.

In this work, metaheuristic methods are applied to balance exploration and exploitation for improving visual trace separation in 3D ICs.

III. Optimization Problem and Metaheuristics

To better visualize the traces of redistribution layers (RDLs) or metal layers in 3D ICs, we formulate color scheme optimization to enhance visual clarity of complex interconnections.

A. Problem Formulation

The color scheme optimization is formulated as a continuous-variable, multi-objective problem, with colors represented in HCL color space as:

$$\mathbf{x} = \{(h_i, c_i, l_i) \mid i = 1, \ldots, n\} \tag{3}$$

where (h_i, c_i, l_i) are HCL color parameters, and n is the total number of colors.

The optimization focuses on the following metrics:

- $\Delta E_{min,inter}$: Minimum inter-group color difference.
- $\Delta E_{min,intra}$: Minimum intra-group color difference.
- $\Delta E_{avg,intra}$: Average intra-group color difference.

The objective is to maximize $\Delta E_{min,inter}$ for inter-group distinction, $\Delta E_{min,intra}$ for sufficient intra-group separation, and $\Delta E_{avg,intra}$ for uniform distribution and visual balance:

$$\begin{aligned} \max F(\mathbf{x}) = {} & w_1\, \Delta E_{min,inter}(\mathbf{x}) \\ & + w_2\, \Delta E_{min,intra}(\mathbf{x}) \\ & + w_3\, \Delta E_{avg,intra}(\mathbf{x}) \end{aligned} \tag{4}$$

where w_1, w_2, and w_3 are predefined weights, and $\mathbf{x}$ denotes the set of color codes.

The three metrics are defined as:

$$\Delta E_{\text{min,inter}}(\mathbf{x}) = \min_{\substack{i \in g,\, j \in g' \\ g \neq g'}} \Delta E(\mathbf{x}_i, \mathbf{x}_j) \tag{5}$$

$$\Delta E_{\text{min,intra}}(\mathbf{x}) = \min_{g \in G} \min_{\substack{i,j \in g \\ i \neq j}} \Delta E(\mathbf{x}_i, \mathbf{x}_j) \tag{6}$$

$$\Delta E_{\text{avg,intra}}(\mathbf{x}) = \frac{1}{|G|} \sum_{g \in G} \frac{2}{|g|(|g|-1)} \sum_{\substack{i<j \\ i,j \in g}} \Delta E(\mathbf{x}_i, \mathbf{x}_j) \tag{7}$$

where $\Delta E(\mathbf{x}_i, \mathbf{x}_j)$ is the color difference between two colors, and G denotes the set of color groups.

Constraints are imposed to enhance perceptual distinguishability and guarantee safe HCL-to-sRGB mapping, where HCL color space is partitioned into regions bounded for each color group g:

$$\begin{aligned} (h_i, c_i, l_i) \in & [h_g^{\min}, h_g^{\max}] \\ & \times [c_g^{\min}, c_g^{\max}] \\ & \times [l_g^{\min}, l_g^{\max}], \quad \forall i \in g \end{aligned} \tag{8}$$

B. Conventional Metaheuristics

Metaheuristics, also known as intelligent optimization algorithms, address optimization problems by searching for optimal or near-optimal solutions [14].

1) Differential Evolution

Differential Evolution (DE) is a population-based metaheuristic on real-valued vectors, using mutation, crossover, and selection [15].

Given a population of n individuals $\mathbf{x}_i$ $(i = 1, \ldots, n)$, each representing a candidate solution, the mutation operator generates a mutant vector:

$$\mathbf{v}_i = \mathbf{x}_{r1} + F \cdot (\mathbf{x}_{r2} - \mathbf{x}_{r3}) \tag{9}$$

where $r1, r2, r3 \in \{1, \ldots, n\}$ are distinct indices different from i, and $F \in [0, 1]$ controls the mutation strength.

The crossover operator combines the target vector $\mathbf{x}_i$ and mutant vector $\mathbf{v}_i$ to produce the trial vector $\mathbf{u}_i$:

$$u_{i,j} = \begin{cases} v_{i,j}, & \text{if } rand_j \leq C_r \text{ or } j = j_{\text{rand}} \\ x_{i,j}, & \text{otherwise} \end{cases} \tag{10}$$

where $p_c \in [0, 1]$ is the crossover probability, $r_j \sim U(0, 1)$, and j_{rand} ensures at least one mutant component is inherited.

Finally, the selection operator retains the better solution for the next generation:

$$\mathbf{x}_i^{(g+1)} = \begin{cases} \mathbf{u}_i, & \text{if } f(\mathbf{u}_i) \leq f(\mathbf{x}_i) \\ \mathbf{x}_i, & \text{otherwise} \end{cases} \tag{11}$$

2) Particle Swarm Optimization

Particle Swarm Optimization (PSO) is inspired by social behavior, where particles update positions based on personal and collective experience [16].

Given a population size n, each particle's position $\mathbf{x}_i$ and velocity $\mathbf{v}_i$ are updated as:

$$\mathbf{v}_i^{t+1} = w\mathbf{v}_i^t + c_1 r_1 (\mathbf{p}_i - \mathbf{x}_i^t) + c_2 r_2 (\mathbf{g}^* - \mathbf{x}_i^t) \tag{12}$$

$$\mathbf{x}_i^{t+1} = \mathbf{x}_i^t + \mathbf{v}_i^{t+1} \tag{13}$$

where w is the inertia weight, c_1, c_2 are cognitive and social coefficients, r_1, $r_2 \sim U(0, 1)$ are uniform random numbers, $\mathbf{p}_i$ is the personal best, and $\mathbf{g}^*$ is the global best.

3) Whale Optimization Algorithm

Whale Optimization Algorithm (WOA) is inspired by the bubble-net hunting behavior of humpback whales [17].

Given a population of n agents, where each agent i represents a candidate solution $\mathbf{x}_i$, positions are updated through three main mechanisms.

First, encircling behavior:

$$\mathbf{x}_i^{t+1} = \mathbf{x}^* - A \cdot D, \quad D = |C \cdot \mathbf{x}^* - \mathbf{x}_i^t| \tag{14}$$

where $\mathbf{x}^*$ is the best solution, and A, C are coefficient vectors.

Second, spiral bubble-net movement:

$$\mathbf{x}_i^{t+1} = D' e^{bl} \cos(2\pi l) + \mathbf{x}^*, \quad D' = |\mathbf{x}^* - \mathbf{x}_i^t| \tag{15}$$

where b is a constant, $l \sim U(-1, 1)$.

Third, random exploration:

$$\mathbf{x}_i^{t+1} = \mathbf{x}_{\text{rand}} - A \cdot D \tag{16}$$

where $\mathbf{x}_{\text{rand}}$ is a randomly selected solution.

4) Grey Wolf Optimizer

Grey Wolf Optimizer (GWO) inspired by the social hierarchy and cooperative hunting behavior of grey wolves [18].

Given a population of n agents, positions are updated based on the top three solutions (α, β, δ wolves), which guide the remaining $n - 3$ agents during the search.

Positions are updated as:

$$\mathbf{X}^{t+1} = \frac{\mathbf{X}_1 + \mathbf{X}_2 + \mathbf{X}_3}{3} \tag{17}$$

where $\mathbf{X}_1$, $\mathbf{X}_2$, $\mathbf{X}_3$ are estimates relative to α, β, and δ. Each estimate is calculated using:

$$\mathbf{X}_m = \mathbf{X}_m^* - A_m \cdot D_m, \quad D_m = |C_m \cdot \mathbf{X}_m^* - \mathbf{X}| \tag{18}$$

where $A_m = 2ar_m - a$ and $C_m = 2r_m$, with $r_m \sim U(0, 1)$ and a linearly decreasing from 2 to 0 over iterations.

5) Cuckoo Search

Cuckoo Search (CS) is inspired by the brood parasitism of certain cuckoo species [19].

Given a population of n nests, new solutions are generated via Lévy flights, enabling occasional long jumps for better exploration [20].

The position update is:

$$\mathbf{x}_i^{(t+1)} = \mathbf{x}_i^{(t)} + \alpha \oplus \text{Lévy}(\lambda) \tag{19}$$

where α is the step size, Lévy(λ) is drawn from a Lévy distribution, and $\oplus$ denotes entry-wise multiplication.

To maintain diversity, a fraction p_a of the worst nests is abandoned and replaced with random solutions.

6) Non-dominated Sorting Genetic Algorithm II

Non-dominated Sorting Genetic Algorithm II (NSGA-II) is an evolutionary algorithm for multi-objective optimization, yielding a Pareto front that reflects objective trade-offs [21].

At each generation, the parent population P_t and the offspring population Q_t are merged into $R_t = P_t \cup Q_t$. Individuals are ranked by non-dominated sorting: the first front contains all non-dominated solutions, the second front contains those dominated only by the first, and so on. Within each front, the crowding distance d_i estimates local density to preserve diversity.

Crossover and mutation are applied using the simulated binary crossover and polynomial mutation operators, with crossover probability p_c and mutation probability p_m, respectively, controlled by distribution indices di_c and di_m.

The next generation P_{t+1} is formed by selecting the top n individuals from R_t based on Pareto rank and crowding distance:

$$P_{t+1} = \text{SelectTop}_n(R_t; \text{Pareto rank}, d_i) \tag{20}$$

where n is the population size, and d_i denotes the crowding distance.

C. Adaptive Elitist Particle Swarm Optimization

We propose Adaptive Elitist Particle Swarm Optimization (AEPSO), an enhanced metaheuristic algorithm that integrates adaptive parameter control, elitism preservation, and whale-inspired spiral search mechanism.

Unlike standard PSO, AEPSO dynamically adjusts inertia weight and acceleration coefficients to balance exploration and exploitation, while preserving the global best solution to avoid quality degradation. A whale-inspired spiral search enhances the ability to escape local optima, and an archive-based leader selection strategy maintains diversity to improve convergence. These mechanisms enable AEPSO to achieve a more effective balance between global exploration and local exploitation, thereby improving optimization performance over conventional PSO.

- Cosine-decayed inertia weight:

$$w(t) = w_{\min} + (w_{\max} - w_{\min}) \cdot \frac{1 + \cos\left(\frac{\pi t}{T}\right)}{2} \tag{21}$$

  where $w_{\min} = 0.2$, $w_{\max} = 0.9$, t is the current iteration, and T is the maximum number of iterations.
- Dynamic acceleration coefficients:

$$c_1(t) = c_1^{\text{start}} - (c_1^{\text{start}} - c_1^{\text{end}}) \cdot \frac{t}{T} \tag{22}$$

$$c_2(t) = c_2^{\text{start}} + (c_2^{\text{end}} - c_2^{\text{start}}) \cdot \frac{t}{T} \tag{23}$$

  where $c_1^{\text{start}} = 2.5$, $c_1^{\text{end}} = 0.5$, $c_2^{\text{start}} = 0.5$, $c_2^{\text{end}} = 2.5$, t is the current iteration, and T is the maximum number of iterations.
- Elitism mechanism: The global best solution g^* is preserved by replacing the worst-performing particle in each generation.
- Whale-inspired spiral search:

$$\boldsymbol{x}_i(t+1) = |\boldsymbol{D}| e^{bl} \cos(2\pi l) + \boldsymbol{g}^* \tag{24}$$

  where $\boldsymbol{D} = |\boldsymbol{g}^* - \boldsymbol{x}_i(t)|$ is the distance between particle i and the global best $\boldsymbol{g}^*$, $b = 1$ controls the spiral shape, and $l \sim U(-1, 1)$ is a uniform random number introducing stochasticity.
- Archive-based leader selection: An archive of non-dominated solutions is maintained, with leaders dynamically selected based on crowding distance to balance convergence and diversity.

IV. 3D Prototype Modeling for Trace Coloring

To construct a 3D prototype model of the chip, we first performed an X-ray scan on an test vehicle using a Zeiss VersaXRM X-ray microscope. The test vehicle is a wire-bond packaged field-programmable gate array (FPGA), measuring 18 × 18 mm, was imaged at an energy level of 70 keV, capturing a stack of 171 high-resolution 2D X-ray images with a voxel size of 2.2 μm using a 4× objective lens.

Following X-ray scanning, a focus stacking process was applied to the image stack, where adjacent images were combined for each circuit layer. This step compensated for the inherent curvature of the chip packaging and enhanced the clarity and precision of each layer's visualization [22], [23]. The reconstruction focused on Layers 2, 3, and 4, which primarily contain the substrate RDLs. Layer 1, used for wire bonding, was excluded. Specifically, 8, 10, and 9 images were stacked for Layers 4, 3, and 2, respectively.

Subsequent to focus-stacking, the detailed geometries of power planes, circuit traces, design rules, and 3D via connections were manually traced and reconstructed using EasyEDA software. Layers 4, 3, and 2 were then stacked and connected using vias in ANSYS High Frequency Structure Simulator (HFSS) to form a 3D prototype model (Fig. 1).

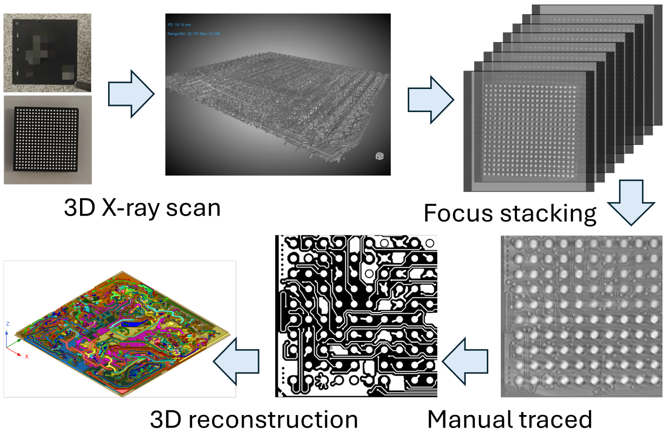

Figure 1. Workflow from X-ray scanning of the test vehicle to the reconstruction of the 3D prototype model.

V. Color Scheme Strategies

We apply nine coloring strategies to the chip model: one clustering-based method, seven metaheuristic methods and one manual design.

In this work, HCL color space is divided into several groups based on hue, and the number of required colors in each group can be defined according to the specific needs of a chip design. The chip model used in this paper consists of six functional regions, each assigned to a designated color group with the following number of required colors:

- **Voltage Common Collector (VCC)** – Red (14 colors)
- **Ground (GND)** – Blue (3 colors)
- **User Input/Output (IO) Pins** – Orange (2 colors)
- **Dedicated Pins** – Green (14 colors)
- **Multi-Function Pins** – Cyan (5 colors)
- **Processing System Multiplexed Input/Output (PS MIO) Pins** and **Processing System Double Data Rate (PS DDR) Pins** – Purple (23 colors)

Bounds for these color groups are defined through segment classification with refined hue specifications [24], assigning each a distinct perceptually constrained color range, as summarized in Table I.

Table I
Hue, Chroma, and Lightness Ranges for Each Color Group

Color Group	Hue ($h°$)	Chroma (c)	Lightness (l)
Red	$[0°, 30°]$	$[50, 80]$	$[40, 70]$
Orange	$[30°, 44°]$	$[55, 80]$	$[50, 75]$
Green	$[100°, 160°]$	$[45, 70]$	$[50, 80]$
Cyan	$[160°, 200°]$	$[50, 75]$	$[60, 85]$
Blue	$[210°, 250°]$	$[50, 75]$	$[40, 75]$
Purple	$[270°, 330°]$	$[50, 80]$	$[35, 70]$

All ΔE_{00} evaluations were carried out in HCL color space using the D65 illuminant and the CIE 2° standard observer. For the eight computer-automated methods, each algorithm was executed 30 times, and the mean and standard deviation were computed for robust evaluation. All experiments were conducted on Ubuntu 24.04.1 LTS with an AMD Ryzen 9 7950X and 8 GB RAM.

A. Clustering-based Method

K-means [25], a widely used clustering algorithm, is employed as the baseline. A post-clustering $\Delta E_{min,intra}$ filter is applied to ensure intra-group separation by repeating clustering until all pairs satisfy the minimum threshold, which linearly decreases from 7.0 to 0 across successive attempts.

B. Metaheuristic Methods

The optimization objective for all metaheuristics is defined in (4).

Most metaheuristic algorithms depends on parameter settings which affect the performance of the algorithms. Table II summarizes the parameter settings used in this paper. To ensure fairness, parameter settings are mainly based on classical literature or original recommendations, minimizing tuning bias across algorithms.

DE and PSO follow [26], GWO and WOA use the original authors' recommended settings [17, 18], and CS is based on [14]. For DE, PSO, WOA, GWO, CS, and AEPSO, the objective weights $w_1 = 0.4$, $w_2 = 2.0$, and $w_3 = 0.1$ are adopted, placing greater emphasis on maximizing $\Delta E_{min,intra}$ to ensure sufficient perceptual separation.

In contrast, NSGA-II employs equal weights $w_1 = w_2 = w_3 = 1$ to explore a well-distributed Pareto front without predefined preferences, and follows the implementation described in [21]. All Pareto-optimal solutions can be retained for user-driven selection. In this study, to emphasize intra-group separability and enable fair comparison with single-solution metaheuristics, we further rank the first front and select the solution with the maximum $\Delta E_{min,intra}$, as illustrated in Fig. 2.

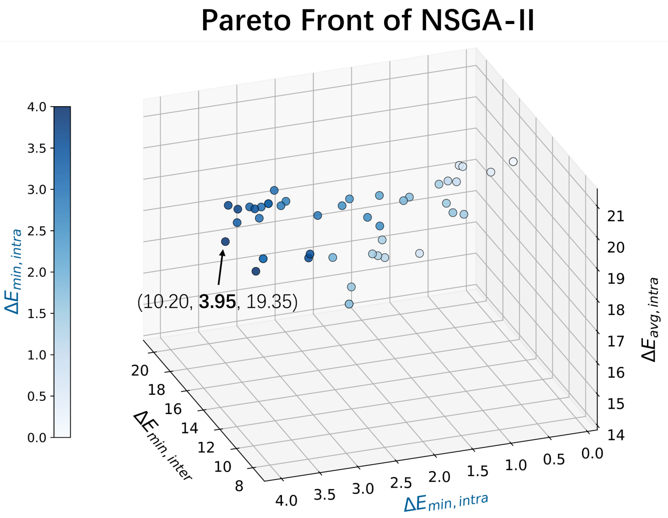

Figure 2. The Pareto front obtained by NSGA-II illustrates the trade-offs among $\Delta E_{min,inter}$, $\Delta E_{min,intra}$, and $\Delta E_{avg,intra}$. Each point denotes a non-dominated solution, with color intensity scaled by $\Delta E_{min,intra}$. While all solutions are viable candidates, this study selects the highlighted point with the maximum $\Delta E_{min,intra}$ of 3.95 to ensure intra-group separability and enable comparison with single-solution metaheuristics.

C. Manual Design

For manual design, a standard RGB-based color wheel, the Adobe Color Wheel [27], is employed to define the boundary colors. Additional colors are generated by varying hue, chroma, and lightness within the defined ranges, resulting in a color scheme with approximately uniform perceptual differences.

D. Visualization in Virtual Reality

Unlike traditional software, virtual reality facilitates immersive spatial learning beyond keyboard-and-mouse interaction [28].

This work extends that paradigm to instructional contexts, building on Ragan et al.'s VR-based spatial inspection of

Table II
PARAMETERS SETTING FOR METAHEURISTIC ALGORITHMS

DE	PSO	WOA	GWO	CS	NSGA-II	AEPSO
$n = 50$ $p_c = 0.7$ $F = 0.6$	$n = 50$ w linearly decreasing from 0.9 to 0.2 $c_1 = 2$ $c_2 = 2$	$n = 50$	$n = 50$	$n = 50$ $\alpha = 1$ $p_a = 0.25$	$n = 100$ $p_c = 0.9$ $p_m = 1/D$ $di_c = 20$ $di_m = 100$	$n = 50$ archive size $= 20$

complex 3D structures [29]. Multilayer substrate visualization is similar to underground cave systems, where detecting small spatial mismatches parallels tasks in modern FA tasks.

The VR environment is developed, where users rotate the substrate with a joystick and use a controller ray to select and highlight VCC parts, which can be pulled out for detailed inspection of shape and color, as shown in Fig. 3.

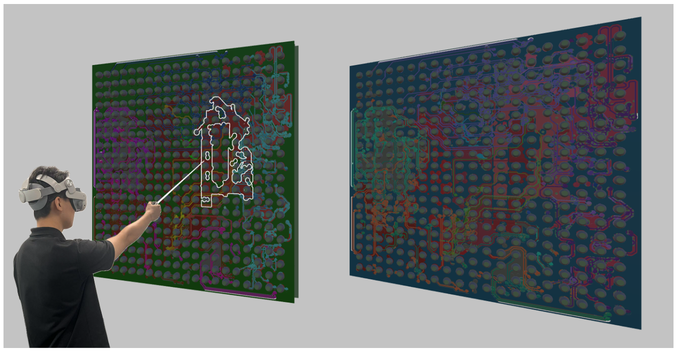

Figure 3. User interact with substrate visualization using hand controllers in a virtual reality environment.

VI. RESULTS AND DISCUSSION

This section presents results for all color scheme strategies, an adaptability analysis of the metaheuristic framework, and a method for handling color vision deficiency.

A. Results for Optimized Color Schemes

The performances of all methods are summarized in Table III. AEPSO achieves the highest mean $\Delta E_{min,intra}$ of 5.52, representing a 24.6% improvement over PSO, the best-performing conventional metaheuristic. In contrast, WOA consistently shows the weakest performance, while DE, GWO, and CS yield moderate improvements and NSGA-II achieves competitive but still inferior results compared to AEPSO. Manual design provides the largest inter-group separation but fails to maintain sufficient intra-group distinction, underscoring the difficulty of balancing these objectives without algorithmic optimization.

Execution time is an important indicator of computational efficiency. As shown in Table III, K-means is the fastest due to its low complexity, whereas metaheuristics incur longer runtimes mainly from repeated pairwise ΔE evaluations. PSO and WOA are relatively efficient, DE and GWO show moderate overhead, CS is slower, and NSGA-II is the most time-consuming. AEPSO requires a slightly higher average runtime than PSO but achieves a favorable efficiency–performance trade-off through enhanced optimization results.

The convergence behavior of $\Delta E_{min,intra}$ across 100 iterations is illustrated in Fig. 4. AEPSO consistently outperforms all methods, showing rapid and stable improvements from the early stages. PSO is the next-best performer, surpassing other methods after iteration 40 with robust upward trends. CS and DE remain relatively stable across iterations, GWO improves gradually, and WOA plateaus early, showing minimal gains thereafter.

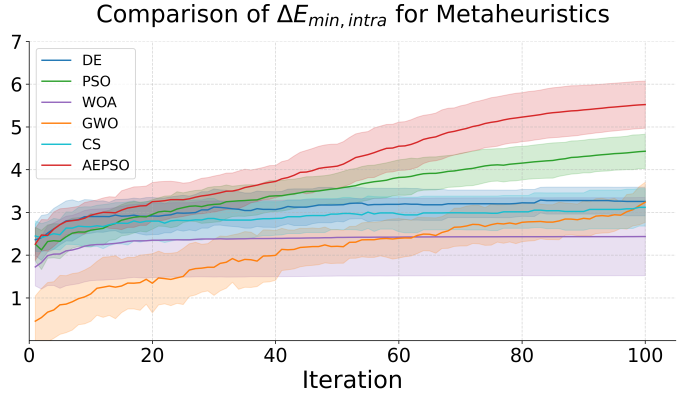

Figure 4. Comparison of $\Delta E_{min,intra}$ over 100 iterations for DE, PSO, WOA, GWO, CS, and AEPSO. The curves show the mean values across 30 runs, with shaded areas indicating standard deviation. AEPSO achieves the highest $\Delta E_{min,intra}$ (5.52 ± 0.55).

Based on the evaluation results, AEPSO is selected to generate the color scheme in Fig. 5, due to its superior overall performance. Two colored 3D chip models using the AEPSO-optimized scheme and the manually designed scheme are presented in Fig. 6, respectively. Red groups from both approaches are further compared in Table IV, highlighting the specific colors assigned to various VCC power rails, with the corresponding red color schemes illustrated in Fig. 7.

B. Adaptability Analysis

We further examined the case where all functional groups were constrained to 23 colors, with group boundaries and optimization settings unchanged. All metaheuristics showed degraded $\Delta E_{min,intra}$ due to the large number of required colors within groups, and none of the conventional metaheuristics exceeded the JND threshold of 2.3. Nevertheless, AEPSO still achieved a mean $\Delta E_{min,intra}$ of 2.47, highlighting its

Table III
Comparison of results across color scheme strategies

Methods	$\Delta E_{min,inter}$	$\Delta E_{min,intra}$	$\Delta E_{avg,intra}$	Time (s)
K-means	8.01 ± 0.36	3.81 ± 0.39	13.37 ± 0.53	176.45
DE	11.79 ± 1.57	3.26 ± 0.33	16.43 ± 1.69	525.70
PSO	16.45 ± 1.79	4.43 ± 0.40	13.90 ± 1.52	516.96
WOA	14.26 ± 6.25	2.44 ± 0.91	12.16 ± 3.85	518.05
GWO	14.39 ± 1.84	3.24 ± 0.47	14.22 ± 1.23	522.49
CS	9.69 ± 1.77	3.12 ± 0.44	16.71 ± 1.21	661.81
NSGA-II	11.91 ± 2.95	3.96 ± 0.25	18.86 ± 1.72	1150.00
AEPSO	14.20 ± 1.96	$\mathbf{5.52 \pm 0.55}$	15.95 ± 1.92	536.54
Manual	54.23	1.51	16.25	N/A*

* Average execution time not applicable to manual design.

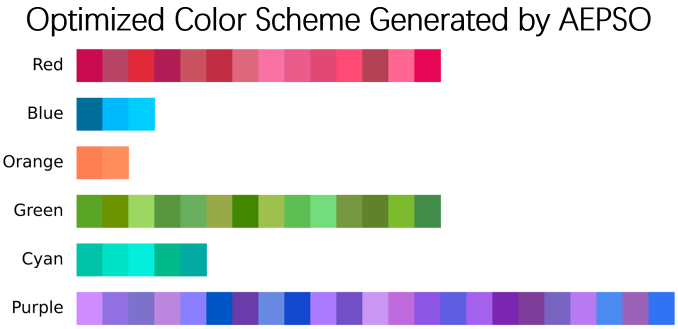

Figure 5. The optimized color scheme for the 3D chip model was generated by metaheuristic methods using AEPSO.

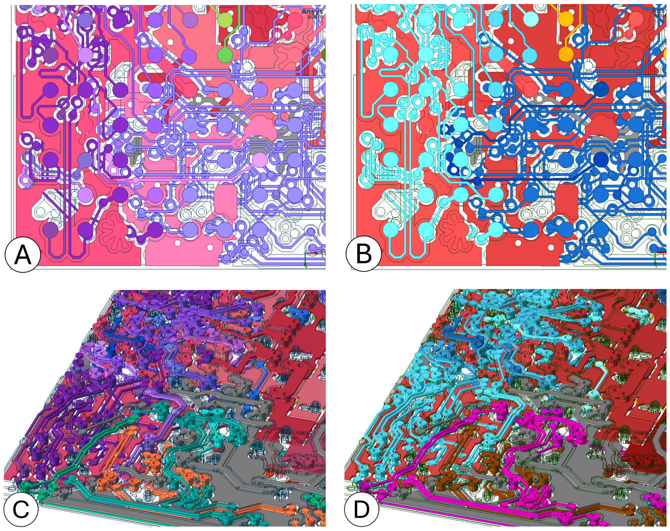

Figure 6. Partial representation of the colored 3D chip model applying different color strategies: (a) AEPSO-optimized color scheme viewing along the $-Z$ axis.; (b) manually selected color scheme viewing along the $-Z$ axis; (c) AEPSO-optimized color scheme viewing along the trimetric orientation; (d) manually selected color scheme viewing along the trimetric orientation.

robustness in maintaining perceptual separability under stringent constraints, as shown in Table V. A resulting palette and intra-group ΔE for each color group are illustrated in Fig. 8.

If different chip tpyes consist more than six functional groups, HCL color space should be re-partitioned to allocate each group a distinct subregion, thereby demonstrating that the proposed metaheuristic framework is readily adaptable to diverse IC layouts.

Table IV
Red Groups of Color schemes Generated by AEPSO and Manual Design

VCC	AEPSO				Manual
	h°	c	l	RGB	RGB
VCCAUX_IO	15.29	71.20	46.15	(209, 24, 82)	(147, 13, 13)
VCCAUX	7.78	50.11	48.89	(191, 74, 107)	(155, 20, 20)
VCCINT	24.16	79.08	41.68	(200, 0, 51)	(163, 27, 27)
VCCO_#	24.90	55.34	46.73	(189, 67, 75)	(172, 33, 33)
VCCBRAM	17.02	56.96	49.99	(202, 70, 94)	(180, 40, 40)
VCCPINT	10.23	56.71	56.15	(222,104,120)	(188, 47, 47)
VCCPAUX	69.59	55.16		(234, 60, 135)	(197, 53, 53)
VCCO_MIO0	0.78	65.50	63.38	(254, 93, 155)	(205, 60, 60)
VCCO_MIO1	8.02	72.73	51.66	(228, 40, 110)	(213, 67, 67)
VCCO_DDR	0.00	54.11	58.53	(223, 95, 143)	(222, 73, 73)
VCCPLL	15.17	58.18	40.00	(175, 37, 73)	(230, 80, 80)
RSVDVCC	17.99	70.01	53.95	(231, 61, 96)	(238, 87, 87)
VCCADC_0	13.07	74.48	62.83	(255, 78, 126)	(247, 93, 93)
VCCBATT_0	4.10	74.17	69.12	(255, 97, 163)	(255,100,100)

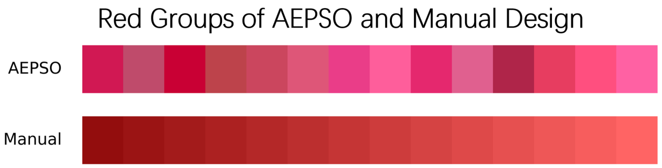

Figure 7. Comparison of red group color schemes generated by AEPSO and manual design for the 3D chip model.

In addition, as heterogeneous integration packaging advances, interconnections emerge not only between packages but also between individual dies [30]. This necessitates coloring the traces and solder bumps that connect these components, constituting an emerging research topic with strong industrial relevance.

As 3D ICs continue to scale, the number of distinguishable colors within a single color space will eventually become insufficient to ensure pairwise separation. In such cases, a new coloring strategy may be adopted: given that interconnects are

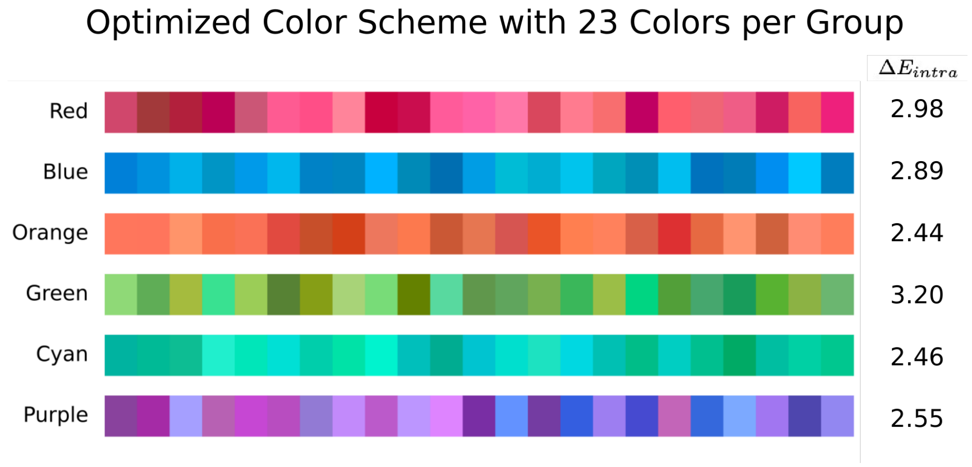

Figure 8. The optimized color scheme with 23 colors per group generated by AEPSO. The metric ΔE_{intra} denotes the minimum color difference within each color group, reflecting intra-group separability.

Table V
COMPARISON OF RESULTS WITH 23 COLORS PER FUNCTIONAL GROUP

Methods	$\Delta E_{min,inter}$	$\Delta E_{min,intra}$	$\Delta E_{avg,intra}$
K-means	4.95 ± 0.29	2.01 ± 0.13	13.33 ± 0.04
DE	5.36 ± 1.57	1.44 ± 0.27	15.38 ± 0.63
PSO	9.58 ± 1.89	1.93 ± 0.26	11.86 ± 0.96
WOA	27.85 ± 6.10	0.16 ± 0.29	2.73 ± 2.74
GWO	9.75 ± 1.40	1.60 ± 0.15	13.27 ± 0.53
CS	3.91 ± 1.38	1.48 ± 0.29	16.36 ± 0.72
NSGA-II	6.62 ± 2.09	2.00 ± 0.12	16.32 ± 0.88
AEPSO	8.25 ± 1.57	$\mathbf{2.47 \pm 0.26}$	13.99 ± 1.06

constrained in length for electrical performance and can thus be clustered within localized regions, a conditional application of a "Four Color Theorem in 3D" can be envisioned, where colors are reused across spatially separated clusters without compromising visual clarity.

C. Color Vision Deficiency Scenarios

Color vision deficiency (CVD) is modeled using the physiologically-based linear transformation matrices [31], which simulate different types of color vision deficiency in the linear sRGB space.

To generate color schemes that remain distinguishable for color-deficient observers, each candidate palette is evaluated under both normal and CVD conditions during the metaheuristic search by projecting the transformed colors into HCL color space, while the objective function enforces intra-group separation and maximizes inter-group distinctness across all scenarios.

CONCLUSION

In this work, we compared seven metaheuristic color scheme strategies to enhance perceptual clarity and trace discrimination in 3D ICs. The proposed AEPSO algorithm achieved the best performance, with a $\Delta E_{min,intra}$ of 5.52, surpassing the JND threshold of 2.3 and ensuring clear intra-group distinction. These findings establish a solid baseline for perceptually meaningful color partitioning in complex IC layouts, applicable to both empirical and simulated structures [5].

A VR environment for immersive inspection and FA was also developed. Future work will include user studies in VR to quantitatively assess perceptual effectiveness and refine color schemes in a human-centered manner. We will also address gamut clipping in HCL-to-sRGB conversion to preserve perceptual separability.

ACKNOWLEDGMENT

This research is supported by A*STAR under its RIE2025 Manufacturing, Trade and Connectivity (MTC) Industry Alignment Fund – PrePositioning (IAF-PP) (Award M22K8a0048). Any opinions, findings, conclusions or recommendations expressed in this material are those of the authors and do not reflect the views of the A*STAR.

This research is supported by the National Research Foundation, Singapore (NRF) under NRF's Medium Sized Centre: Singapore Hybrid-Integrated Next-Generation μ-Electronics (SHINE) Centre funding programme.

REFERENCES

[1] J. Hong, R. Hnatyshyn, E. A. Santos, R. Maciejewski, and T. Isenberg, "A survey of designs for combined 2d+3d visual representations", *IEEE Transactions on Visualization and Computer Graphics*, vol. 30, no. 6, pp. 2888–2902, Jun. 2024. DOI: 10.1109/tvcg.2024.3388516.

[2] Y. Gao, J. Liang, and J. Yang, "Color palette generation from digital images: A review", *Color Research & Application*, vol. 50, no. 3, pp. 250–265, Dec. 2024. DOI: 10.1002/col.22975.

[3] S. S. Iyer, "Heterogeneous integration for performance and scaling", *IEEE Transactions on Components, Packaging and Manufacturing Technology*, vol. 6, no. 7, pp. 973–982, Jul. 2016. DOI: 10.1109/tcpmt.2015.2511626.

[4] G. Sharma, *Digital Color Imaging Handbook*. CRC Press, 2003.

[5] Z. Shi, L. Lum, B. Zee, J. M. Chin, and Y. K. Lim, "First proof of 3d-ic power plane defect localization via frequency domain spatial heat mapping", *2025 IEEE 75th Electronic Components and Technology Conference (ECTC)*, pp. 1153–1159, May 2025. DOI: 10.1109/ectc51687.2025.00199.

[6] G. H. Joblove and D. Greenberg, "Color spaces for computer graphics", *ACM SIGGRAPH Computer Graphics*, vol. 12, no. 3, pp. 20–25, Aug. 1978. DOI: 10.1145/965139.807362.

[7] M. Anderson, R. Motta, S. Chandrasekar, and M. Stokes, “Proposal for a standard default color space for the internet—srgb”, *Color and Imaging Conference*, vol. 4, no. 1, pp. 238–245, Jan. 1996. DOI: 10.2352/cic.1996.4.1.art00061.

[8] Y. Ohno, “Cie fundamentals for color measurements”, in *NIP & Digital Fabrication Conference*, Society of Imaging Science and Technology, vol. 16, 2000, pp. 540–545. DOI: 10.2352/ISSN.2169-4451.2000.16.1.art00033_2.

[9] Commission Internationale de l’Éclairage (CIE), “Colorimetry”, Division 1, Central Bureau of the CIE, Vienna, Austria, Tech. Rep. CIE 015:2018, 2018. DOI: 10.25039/TR.015.2018.

[10] M. R. Luo, G. Cui, and B. Rigg, “The development of the cie 2000 colour-difference formula: Ciede2000”, *Color Research & Application*, vol. 26, no. 5, pp. 340–350, Aug. 2001. DOI: 10.1002/col.1049.

[11] J. Albers, *Interaction of color*. Yale University Press, 2013.

[12] L. Eiseman and K. Recker, *Pantone: the twentieth century in color*. Chronicle Books, 2011.

[13] J. Delon, A. Desolneux, J. L. Lisani, and A. B. Petro, “Automatic color palette”, in *IEEE international conference on image processing 2005*, IEEE, vol. 2, 2005, pp. II–706. DOI: 10.1109/ICIP.2005.1530153.

[14] X.-S. Yang, “Nature-inspired mateheuristic algorithms: Success and new challenges”, *Journal of Computer Engineering and Information Technology*, vol. 01, no. 01, 2012. DOI: 10.4172/2324-9307.1000e101.

[15] R. Storn and K. Price, “Differential evolution–a simple and efficient heuristic for global optimization over continuous spaces”, *Journal of global optimization*, vol. 11, no. 4, pp. 341–359, 1997. DOI: 10.1023/A:1008202821328.

[16] J. Kennedy and R. Eberhart, “Particle swarm optimization”, in *Proceedings of ICNN’95-international conference on neural networks*, ieee, vol. 4, 1995, pp. 1942–1948. DOI: 10.1109/ICNN.1995.488968.

[17] S. Mirjalili and A. Lewis, “The whale optimization algorithm”, *Advances in engineering software*, vol. 95, pp. 51–67, 2016. DOI: 10.1016/j.advengsoft.2016.01.008.

[18] S. Mirjalili, S. M. Mirjalili, and A. Lewis, “Grey wolf optimizer”, *Advances in engineering software*, vol. 69, pp. 46–61, 2014. DOI: 10.1016/j.advengsoft.2013.12.007.

[19] X.-S. Yang and S. Deb, “Cuckoo search via lévy flights”, in *2009 World congress on nature & biologically inspired computing (NaBIC)*, Ieee, 2009, pp. 210–214. DOI: 10.1109/NABIC.2009.5393690.

[20] R. N. Mantegna, “Fast, accurate algorithm for numerical simulation of levy stable stochastic processes”, *Physical Review E*, vol. 49, no. 5, p. 4677, 1994. DOI: 10.1103/PhysRevE.49.4677.

[21] K. Deb, A. Pratap, S. Agarwal, and T. Meyarivan, “A fast and elitist multiobjective genetic algorithm: Nsga-ii”, *IEEE transactions on evolutionary computation*, vol. 6, no. 2, pp. 182–197, 2002. DOI: 10.1109/4235.996017.

[22] A. Phoulady, Y. Suleiman, H. Choi, N. May, S. Shahbazmohamadi, and P. Tavousi, “Automated 3d semantic segmentation of pcb x-ray ct images and netlist extraction”, *Scientific Reports*, vol. 15, no. 1, Jan. 2025. DOI: 10.1038/s41598-024-84635-2.

[23] C. Xi, A. A. Khan, J. True, N. Vashistha, N. Jessurun, and N. Asadizanjani, “Digital twin aided ic packaging structure analysis for high-quality sample preparation”, *2021 IEEE International Symposium on the Physical and Failure Analysis of Integrated Circuits (IPFA)*, pp. 1–6, Sep. 2021. DOI: 10.1109/ipfa53173.2021.9617431.

[24] S. D. Smith, “Quantifying color variation: Improved formulas for calculating hue with segment classification”, *Applications in plant sciences*, vol. 2, no. 3, p. 1 300 088, 2014. DOI: 10.3732/apps.1300088.

[25] J. B. McQueen, “Some methods of classification and analysis of multivariate observations”, in *Proc. of 5th Berkeley Symposium on Math. Stat. and Prob.*, 1967, pp. 281–297.

[26] M. Swamy, *Search and Optimization by Metaheuristics-Techniques and Algorithms Inspi*. Birkhauser Verlag Ag, 2016.

[27] *Adobe color wheel*, https://color.adobe.com/create/color-wheel, Accessed: 2025-07-17, Adobe Inc.

[28] T. Lin *et al.*, “Aromacanvas: A wearable olfactory display for chinese painting appreciation and learning in virtual reality”, *Computers & Education: X Reality*, vol. 7, p. 100 109, 2025. DOI: 10.1016/j.cexr.2025.100109.

[29] E. D. Ragan, R. Kopper, P. Schuchardt, and D. A. Bowman, “Studying the effects of stereo, head tracking, and field of regard on a small-scale spatial judgment task”, *IEEE Transactions on Visualization and Computer Graphics*, vol. 19, no. 5, pp. 886–896, 2013. DOI: 10.1109/TVCG.2012.163.

[30] J. H. Lau, *Chiplet design and heterogeneous integration packaging*. Springer Nature Singapore Springer, 2023.

[31] G. M. Machado, M. M. Oliveira, and L. A. Fernandes, “A physiologically-based model for simulation of color vision deficiency”, *IEEE transactions on visualization and computer graphics*, vol. 15, no. 6, pp. 1291–1298, 2009. DOI: 10.1109/TVCG.2009.113.